Journal of Power Sources 195 (2010) 3316–3322

Contents lists available at ScienceDirect

Journal of Power Sources

journal homepage: www.elsevier.com/locate/jpowsour

Influence of alkali ion doping on the electrochemical performances of tin-based composite materials

A. Aboulaich [a], D.E. Conte [a,*], J. Olivier-Fourcade [a], C. Jordy [b], P. Willmann [c], J.C. Jumas [a]

[a] Institut Charles Gerhardt-Laboratoire des Agrégats, Interfaces et Matériaux pour l'Energie (UMR 5253), Place Eugène Bataillon, 34095 Montpellier Cedex 5, France
[b] SAFT, 111-113 Boulevard Alfred Daney, 33300 Bordeaux Cedex, France
[c] Centre National d'Etudes Spatiales, 18 Avenue Edouard Belin, 31401 Toulouse Cedex 9, France

ARTICLE INFO

Article history:
Received 12 October 2009
Received in revised form
17 November 2009
Accepted 20 November 2009
Available online 27 November 2009

Keywords:
Li-ion
Anodic materials
Tin-based composites
Conductivity

ABSTRACT

In this paper, we report an investigation of three tin-based composite materials as negative electrodes for lithium-ion batteries. Theses composites were synthesized by solid state reaction from dispersion of micrometric tin into BPO_4, Li-doped BPO_4 (LiBPO) and Na-substituted BPO_4 (NaBPO) matrix, respectively. We have investigated more particularly the influence of the two alkaline ions (Li^+, Na^+) introduced into the matrix on electrochemical performances. The morphology of powders was observed by SEM and the composition studied by EDX analysis. The conductivity measurements showed that the modified BPO_4 matrixes (Li or Na) exhibit improved conductivity ($\sigma_{RT} = 2 \times 10^{-11}$ S cm^{-1} for NaBPO). A focus of our interest was to relate the nature and structural composition of the composite interface between active tin and inactive matrix to the irreversible capacity in this type of composite materials. The electrochemical analysis shows a decrease of the irreversible capacity for the composite based on modified matrixes (around 150 and 190 mAh g^{-1} for SnNaBPO and SnLiBPO, respectively) with respect to the reference composite SnBPO (245 mAh g^{-1}).

1. Introduction

Lithium-ion batteries have attracted considerable interest because of their promising applications ranging from electronic devices, electric and hybrid vehicles to even space applications.

Since the first Li-ion cells commercialized by Sony with a Li_xC_6 negative electrode, much research has been undertaken for new anode materials in order to improve the energy density for lithium-ion batteries [1].

The announcement of the *Stalion* battery by Fuji film has stimulated intense discussion on the use of amorphous tin composite oxides (ATCO) as anodic materials [2–4]. The lithium insertion mechanism has been studied by Chouvin et al. and Courtney et al. using ^{119}Sn Mössbauer spectroscopy *ex situ* and *in situ*, respectively [5,6]. The main drawback of these composite materials is the large irreversible capacity (around 660 mAh g^{-1}) due to the formation of Sn^0 from SnO reduction in the first discharge [7,8].

In our past investigations, BPO_4 has been used as inert matrix for dispersion of tin particles [9,10]. This composite shows a higher reversible capacity and a smaller irreversible part with respect to ATCO [8]. In this Paper, we present a new strategy to reduce the irreversible capacity by structural modification of the BPO_4 matrix.

Tin dispersed in amorphous $Na_wB_xP_yO_z$ and crystalline $Li_xB_yPO_z$ matrixes is studied using ^{119}Sn Mössbauer spectroscopy, X-ray diffraction and galvanostatic cycling. EDX coupled SEM imaging has been used to confirm the Sn/matrix interaction.

2. Experimental

The reference compound BPO_4 was synthesized by conventional solid state reaction. The precursors, H_3BO_3 (Acros Organics) and $NH_4H_2PO_4$ (Acros Organics), were homogeneously grinded and the matrix formed by heat treatment (380 °C under air) then slowly cooled down to room temperature (RT). Micrometric Sn (Sigma–Aldrich) was subsequently weighed and added to the previously produced matrix to obtain a composite of average formula $Sn_{0.72}[BPO_4]_{0.28}$. After a 7-h reaction under N_2 flow at 500 °C, the composite was extracted from the oven and quenched to RT. The same procedure has been followed for $Li_xB_yPO_z$ and for $Na_wB_xP_yO_z$. For the former, mono-hydrated LiOH (Prolabo) was added employed along with a more intensive heat treatment (1000 °C under air) also ended in a slow cooling. The stoichiometry of the reagents was calculated for an oxygen deficient compound. Na_2CO_3 (Fluka Biochemika) along with a melt-quenching procedure (850 °C under air) was used for the latter matrix.

* Corresponding author. Tel.: +33 4 67 14 90 99; fax: +33 4 67 14 33 04.
E-mail address: iguanasornione@libero.it (D.E. Conte).

0378-7753/$ – see front matter © 2009 Elsevier B.V. All rights reserved.
doi:10.1016/j.jpowsour.2009.11.094

X-ray diffractograms were recorded using a diffractometer equipped with Cu Kα radiation in the range $10 < 2\theta < 90^\circ$. The FULLPROF [11] software has been used for the profile matching of the $Li_xB_yPO_z$ diffractogram and for the calculation of its unit cell parameters. The quality of the refinement was controlled by the classical χ^2-test.

A Quanta 200F SEM microscope (Fei-Tecnai) equipped with an Oxford Instruments INCA X-sight EDX (Energy-dispersive X-ray) analyzer has been used for imaging and composition confirmations. The SnLiBPO composite has been included into an epoxidic resin in order to obtain a polished surface to observe. A microtome Leica Ultracut UCT with glass knife has been used to obtain a horizontal surface.

^{119}Sn Mößbauer spectra were recorded in transmission geometry with a constant acceleration mode using a conventional EG&G spectrometer. The source was ^{119m}Sn in a $CaSnO_3$ matrix, and spectra were collected at room temperature. The spectra were fitted to Lorentzian profiles by the least-squares method using the WinISO software [12]. The quality of the refinement was controlled here, by the same χ^2-test used for X-rays treatment. Isomer shifts are given with respect to the room temperature spectrum of $BaSnO_3$.

Conductivity measurements were carried on using a Pt|Pt cell linked to a Hewlett-Packard 4192A LF impedance analyzer operating in the frequency range 5 Hz to 13 MHz and in the temperature range 25–550 °C. The compound to be tested was compressed with a pressure of 150 bar in a 1.33-cm^2 round pellet. The thickness of the BPO_4, $Li_xB_yPO_z$ and $Na_wB_xP_yO_z$ pellets was, respectively, 533, 816 and 850 μm. The obtained pellets were compacted by heat treatment under air (800 °C for BPO_4 and $Li_xB_yPO_z$ whereas 400 °C $Na_wB_xP_yO_z$) and then slowly cooled to RT. A circular surface of 0.26 cm^2 was subsequently metallized using a Balzers SCD004 sputter coater equipped with a Pt counter electrode. Impedance spectra were fitted using the ZSimpWin® software.

Electrochemical tests were conducted using Swagelok™ type cells employing lithium foil as a counter electrode, a mixture of 90% active material and 10% carbon black powders as working electrode and utilizing 1 M $LiPF_6$ dissolved in a mixture of organic solvents (EC/PC/DMC 1:1:3, received by SAFT, Bordeaux) as the electrolyte. The assembly was carried out in Ar-filled glove box. The discharge-charge tests were carried out by means of a Mac-Pile system operating in galvanostatic mode, between 1.2 V and 0.01 V vs. Li^+/Li^0 with a cycling speed of alternatively C/8 or C/5 (expressed as 1 Li^+ equivalent inserted/extracted in 8 or 5 h).

3. Results and discussion

3.1. X-ray diffraction

The XRD patterns of the Li-doped BPO_4 (LiBPO) and the Na-substituted BPO_4 matrixes (NaBPO) as well as the corresponding composite materials (SnLiBPO and SnNaBPO) compared with the reference Sn-BPO_4 (SnBPO) composite material are shown in Fig. 1. The Li-doped BPO_4 matrix shows a high crystallinity and all the diffraction lines correspond to BPO_4 as reported in the JCPDS #74-1169. The diffraction peaks can be indexed in the I-*4* space group with the following cell parameters: $a = 4.339(1)$ Å, $c = 6.642(1)$ Å. These results are in agreement with the previously published data [13] indicating a negligible effect of lithium doping on the BPO_4 host crystal structure. The XRD data of Na-substituted BPO_4 shows the absence of long-range order which clearly shows the amorphous nature of this matrix.

After *ex situ* dispersion of micrometric tin into both modified BPO_4 matrixes, the diffraction peaks of β-Sn (JCPDS #86-2265) and BPO_4 appear only for SnLiBPO. Compared to the SnBPO diffraction pattern, the SnLiBPO pattern still retains a certain intensity relative to its matrix diffraction peaks. This is not surprising if one keeps in mind the synthesis conditions of the two matrixes and the quantity of alkaline ions utilized.

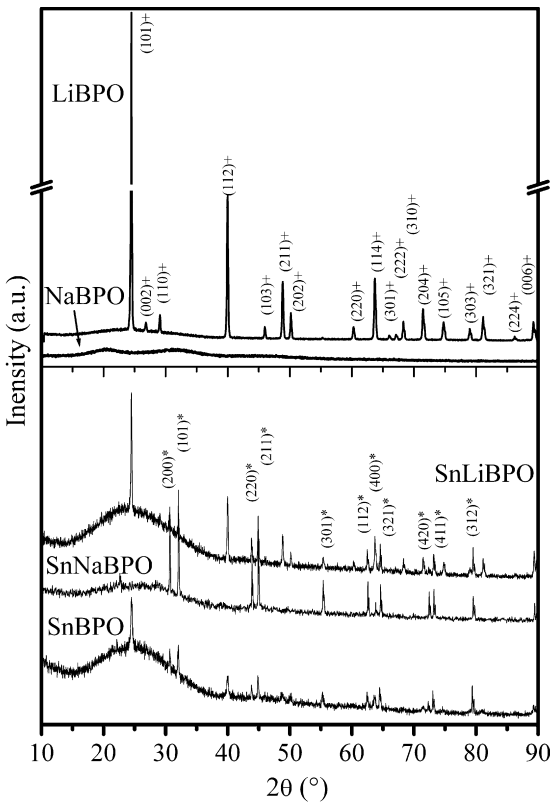

Fig. 1. X-ray diffraction patterns of Li-doped BPO_4 and Na-substituted BPO_4 and of the corresponding composite after dispersion of β-Sn compared with the reference composite SnBPO ($\lambda_{Cu\ K\alpha} = 1.5418$ Å).

The presence of a large diffusion domain in the $20 < 2\theta < 34^\circ$ range can be observed. This has been attributed to the partial amorphisation of the composite [9]. As expected, the SnNaBPO pattern shows only the peaks of β-Sn.

3.2. Scanning electron microscopy–EDX

Fig. 2 shows SEM images and EDX spectra in two different zones of SnLiBPO (as-synthesized, resin included) and SnNaBPO (powder). As visible, the particles vary in size from 20 to 150 μm for SnLiBPO and from 5 to 100 μm for SnNaBPO. The images observed in backscattering mode highlight two different zones; one appears clear (zone 1) and the second appears darker instead (zone 2). The composition of zone 1 in both composites (Table 1) shows a large presence of Sn. In these areas the data are collected on one of the β-Sn particles dispersed during the synthesis step. The presence of the other elements should be attributed to part of the matrix (we stress that EDX is a "3D" analysis which collects data up to 1 μm deep) which can be partially coated by the β-Sn particle. The large excess of oxygen recorded is the product of different compounds: the matrix itself as well as some H_2O vapor adsorbed on the compound or on the carbon adhesive tape, a partial, non-extended oxidation of β-Sn and, in the case of SnLiBPO, the embedding resin.

When moving to zone 2, the presence of tin is largely diminished. This part of the sample is assigned to the matrix itself and to the Sn^{II} based glassy interface (*cfr.* Mößbauer spectroscopy). We recall that matrix diffraction peaks can be seen by XRD measurements (Fig. 1) and that the Sn^{II} based interface has been previously

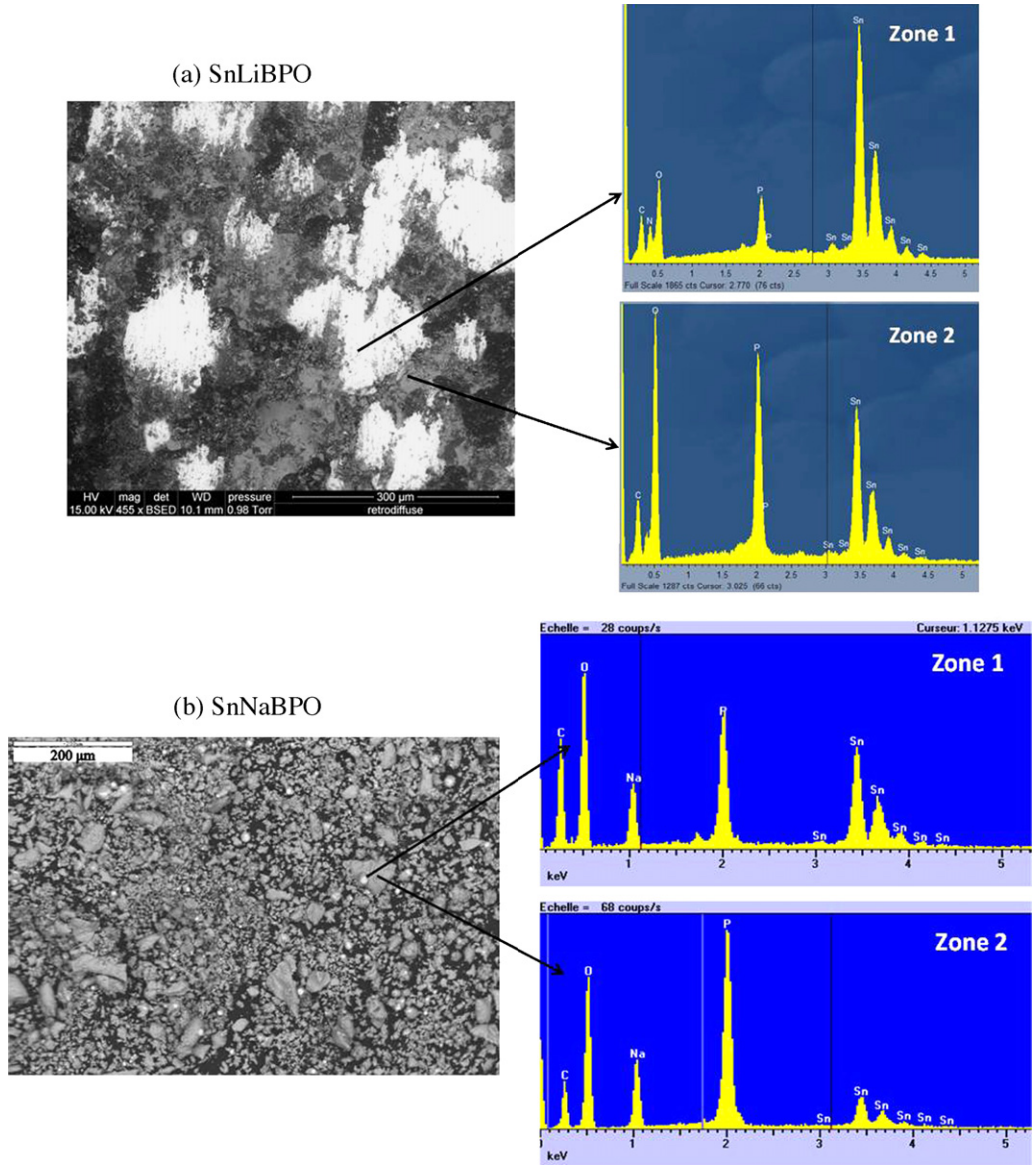

Fig. 2. Scanning electron micrographs and EDX spectra of (a) SnLiBPO and (b) SnNaBPO powders.

Table 1
The EDX results for both SnLiBPO and SnNaBPO composite materials (atomic percentage). The zones selected for analysis were shown in Fig. 2a and b.

Code	Elements	Zone 1	Zone 2
SnLiBPO	Sn	34	12.7
	P	4.4	9.7
	O	61.7	77.5
SnNaBPO	Sn	27.2	11.5
	P	10.7	16.1
	Na	9.2	13.6
	O	52.9	58.1

considered as a glass (Fig. 1 and Ref. [9]). Here again the depth of penetration has to be taken into account.

The amounts of lithium and boron are not indicated due to their light atomic weight which does not permit the analysis of their emitted radiations. In any case this analysis does not permit to separate the extent of pinning effect ("bubbles" appearing on the surface of the tin particle; Fig. 3) with respect to the coating effect (tin part enclosed in the matrix; Fig. 3) after the dispersion of β-Sn. A mix of the two has to be taken into account in order to explain the reciprocal interaction between Sn and the matrix.

3.3. ^{119}Sn Mößbauer spectroscopy

A deeper insight in the local environment of tin atoms can be obtained by ^{119}Sn Mößbauer spectroscopy. Fig. 4 shows both the experimental data and the fitted curves of the Mößbauer spectra recorded at room temperature for SnLiBPO and SnNaBPO compared with the reference composite (SnBPO).

Two components were used to fit all the spectra. One sub-spectrum gives small QS and IS corresponding to metallic tin. The second sub-spectrum gives large QS and IS similar to those previously observed for Sn^{II} [10] and attributed here to the amorphous part observed with XRD. Table 2 presents the Mößbauer parameters obtained from the spectra of the three composite materials.

As discussed in a recent work [8] we chose not to fix the values of hyperfine parameters corresponding to β-Sn ($\delta = 2.56$ mm s^{-1}, $\Delta = 0.29$ mm s^{-1} [14]). Instead we preferred to first evaluate the line width at half-maximum of the Sn^{II} sub-spectrum and then to fix it for the overall treatment of the recorded spectra (this is represented

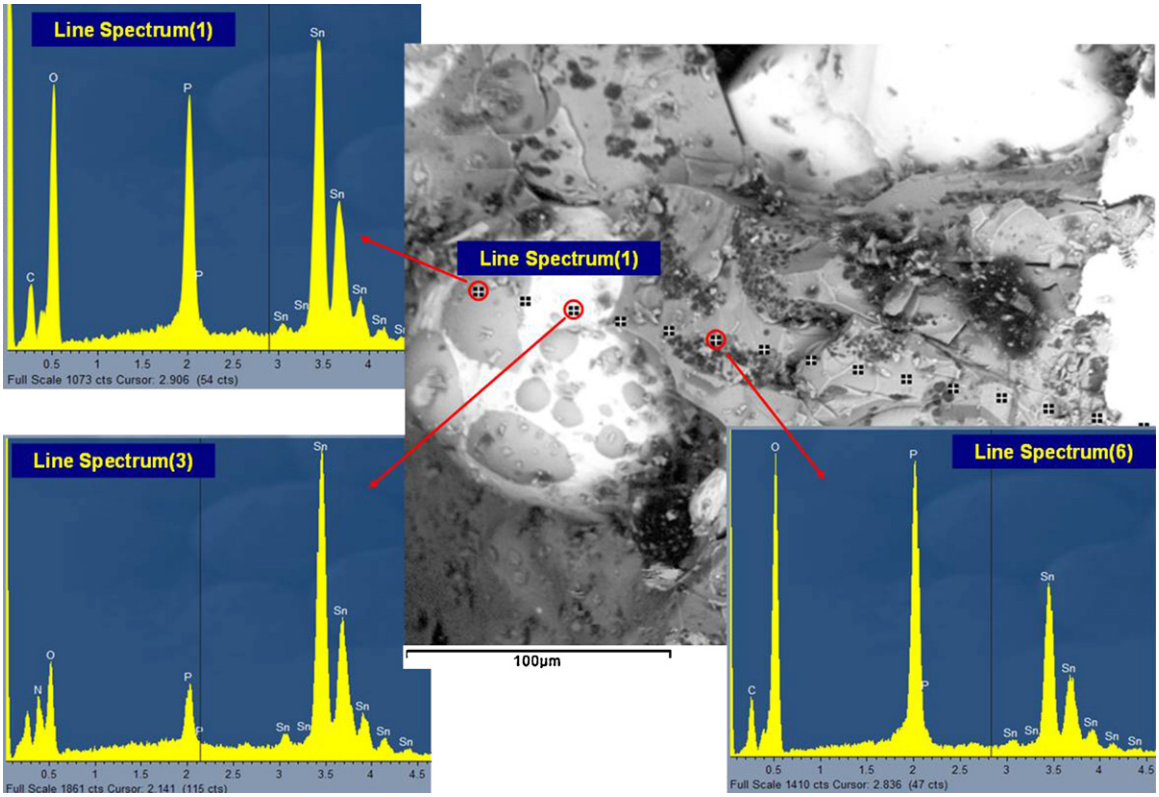

Fig. 3. SEM micrographs and EDX spectra of SnLiBPO in three different points. The mixed effect of both pinning and coating is visible.

by "*" in Table 2). Effective fractions of the two tin species can be directly calculated using the following equation:

$$EF_i = \frac{SF_i/f_i}{\sum_i SF_i/f_i} \quad (1)$$

where SF is the spectral fraction of the analyzed species (given by the relative area of the corresponding sub-spectrum) and f is the Lamb–Mößbauer factor representing the probability of a nuclear transition (absorption or emission) without variation of the vibrational state of the lattice spectrum. The values of f have been previously determined [8] and correspond to $f(Sn^0) = 0.07(1)$ and $f(Sn^{II}) = 0.12(3)$.

Concerning the Sn^{II} contribution, the values of isomer shift and quadrupole splitting of SnLiBPO are close to those of the reference composite SnBPO, while the effective proportion is less important for the composite formed from the Li-doped matrix. This means that the nature of the interface formed between matrix and β-Sn is not changed after doping the BPO_4 matrix by lithium and thus the difference in the amount of interfacial Sn^{II} formed, under the same synthesis conditions, accounts for a difference in the texture of the matrix itself (Fig. 5).

For SnNaBPO sample, the values of hyperfine parameters are quite different. As regards the Sn^{II} species, its variation in isomer shift is due to variations in the Sn 5*s* and/or Sn 5*p* electronic populations. The isomer shift is given by the equation [15]:

$$\delta = \alpha[\rho_a(0) - \rho_s(0)] \quad (2)$$

where $\rho_a(0)$ and $\rho_s(0)$ are the electron densities at the nucleus of the absorber and source respectively while α is a calibration constant. For a qualitative analysis, it is possible to relate δ to the amount of Sn 5*s* and Sn 5*p* electrons of the absorber species by the following equation:

$$\rho_a = cnst + 10N_{5s} - N_{5p} \quad (3)$$

where N_{5s} and N_{5p} are the numbers of Sn 5*s* or Sn 5*p* electrons, respectively.

In the case of Sn^{II}, it is possible to record a decrease in the isomer shift value due either to a decrease in the amount of 5*s* electrons or to an increase in the amount of 5*p* electrons. Considering that sodium is stabilized as a cation in the glass, the rest of the composite material is globally negatively charged. Thus, it is reasonable to consider an increase in the covalency of the Sn–O bonds, reflected in the increase of the 5*p* electrons population in the Sn^{II} specie, respect to the case of the composites formed with crystalline BPO_4 (SnBPO and SnLiBPO). The higher quadrupole splitting (1.81 mm s^{-1}) may also account for a more distorted Sn^{II} geometry.

It is worth noting that a remarkably smaller relative amount of divalent tin is present is this composite compared to other ones (see Table 2). A possible explanation of this effect is probably the presence of large amounts of sodium in the matrix, which renders it already glassy before it is contacted with tin. This phase is probably less reactive than the crystalline BPO_4, this assertion being comforted by the fact that Na^+ and Sn^{2+} have a very similar ionic radius and both react with the crystalline borophosphate as network modifiers to give the glass state. The previous reaction with Na^+ hinders therefore the subsequent reaction of the matrix with tin metal.

3.4. Conductivity measurements

The Arrhenius plot of the conductivity ($\sigma(1/T)$) for the substituted matrixes (LiBPO and NaBPO) is represented in Fig. 6. According the Arrhenius equation:

$$\sigma = \sigma_0 \ \exp\left(\frac{-E_a}{kT}\right) \quad (4)$$

where σ is the material conductivity (obtained by AC impedance response, not showed), σ_0 is a pre-exponential factor characteristic

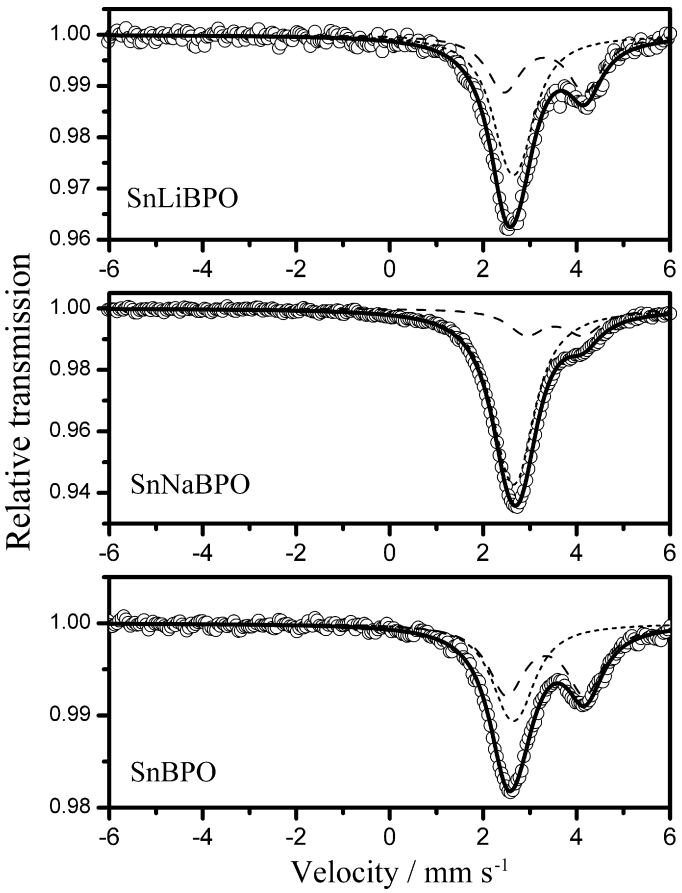

Fig. 4. ^{119}Sn Mößbauer spectra recorded in transmission mode at room temperature for the three composites: SnLiBPO, SnNaBPO and reference SnBPO. Open circles denote the experimental data and the calculated spectrum is denoted by solid bold line. The different contributions to the spectra are denoted by a dotted line for β-Sn, a dashed line for Sn^{II}.

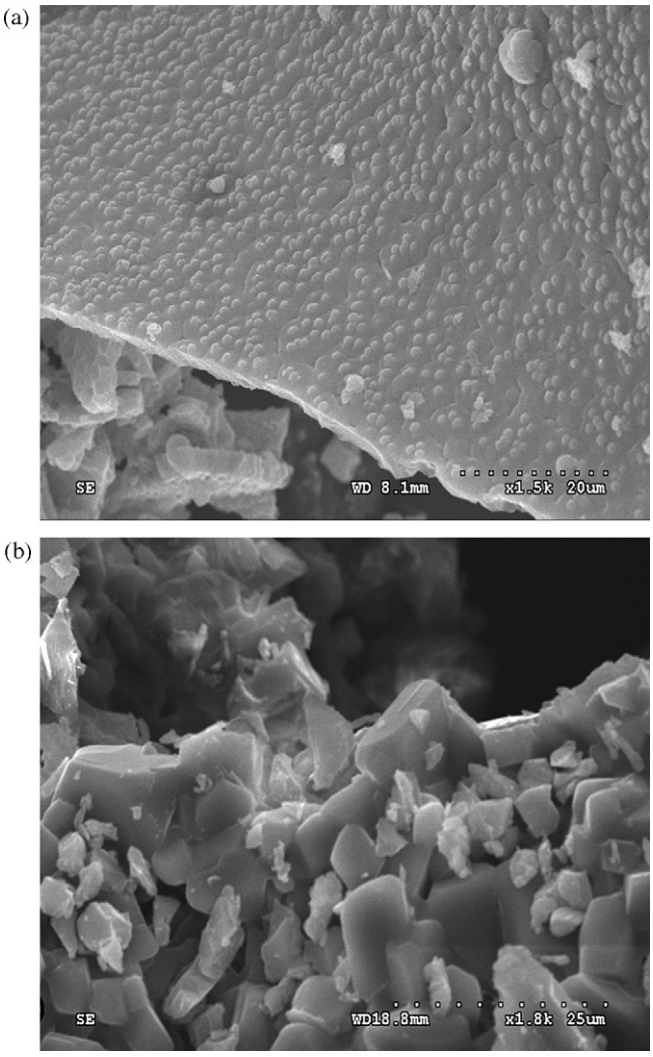

Fig. 5. SEM micrographs of (a) BPO matrix (380 °C) used for the reference compound (SnBPO) and (b) LiBPO matrix (1000 °C).

of the material, E_a is the activation energy of the conduction process, k is the Boltzmann's constant and T the absolute temperature. The activation energy of the process can then be determined from the slope of the Arrhenius plot.

We calculated a value of $E_a = 1.41$ eV for the LiBPO matrix while its extrapolated RT conductivity was calculated to be $\sigma_{(298\,K)} = 8 \times 10^{-22}$ S cm^{-1}. This value is higher respect to SnBPO but is much different from that reported in previous works [16,17] for samples of composition similar to our compound. It is also true that our sample has not been submitted to mechanical milling thus possessing large particle agglomerates of much dispersed sizes (Fig. 5). This can account for a lengthen in the Li^+ diffusion paths with a consequent hindering in the total conductivity. On the other hand, since our initial intention was to produce an under-stoichiometric compound, oxygen conductivity may not be passed over. Activation energies and conductivity values close to ours have been reported by Lanfredi and de Lima Nobre [18] for a pyrochlore type $Bi_3Zn_2Sb_3O_{14}$ ceramic. They attributed such a behavior to a hopping type mechanism for electronic transport suggesting the presence of

Table 2
Hyperfine parameters obtained from ^{119}Sn Mößbauer spectra in transmission mode recorded at room temperature for SnLiBPO, SnNaBPO and SnBPO materials. Isomer shift relative to $BaSnO_3$ "δ" (mm s^{-1}), quadrupole splitting "Δ" (mm s^{-1}), line width at half-maximum "Γ" (mm s^{-1}), relative area of the sub-spectra "S.F." (%), effective fraction "E.F." (%) and refinement quality χ^2. "*" represents fixed values.

Code	δ	Δ	Γ	S.F. %	E.F. %	Site	χ^2
SnLiBPO	2.53(3)	0.33(5)	0.95(4)	61	74	Sn^0	0.42
	3.27(3)	1.64(5)	0.83(*)	39	26	Sn^{II}	
SnNaBPO	2.63(1)	0.21(2)	0.96(1)	82	89	Sn^0	0.47
	3.15(1)	1.81(2)	0.80(*)	18	11	Sn^{II}	
SnBPO	2.51(2)	0.39(3)	0.83(3)	41	56	Sn^0	0.52
	3.27(2)	1.62(3)	0.99(*)	59	44	Sn^{II}	

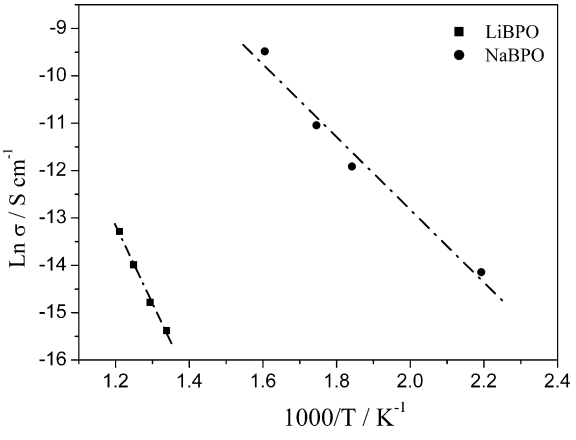

Fig. 6. Arrhenius plot for LiBPO and NaBPO.

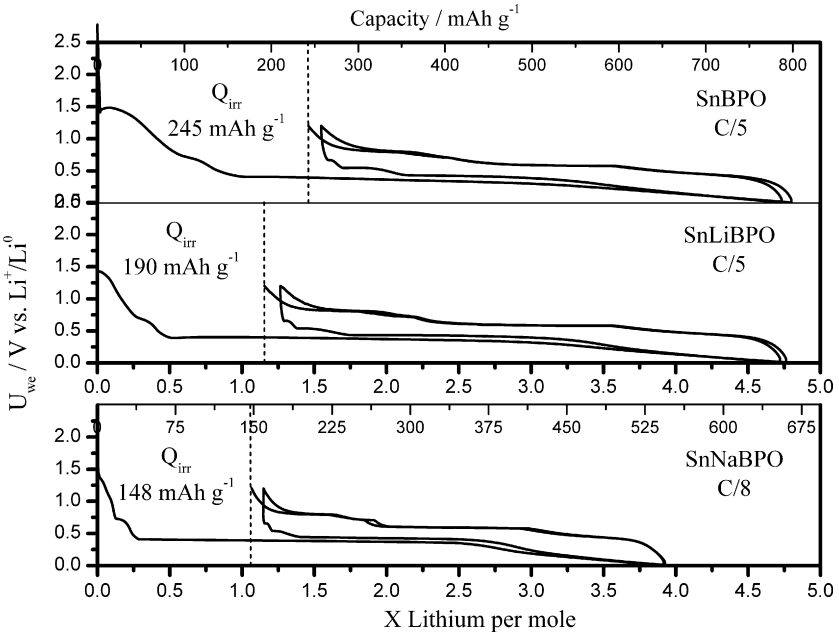

Fig. 7. Galvanostatic cycling curves at C/5 of SnBPO, SnLiBPO and at C/8 of SnNaBPO in the potential window between 0.01 V and 1.2 V vs. Li^+/Li^0.

O^{2-} vacancies in the lattice. A more accurate study in this direction is currently undertaken.

As regards the NaBPO sample, its calculated activation energy value is lower (E_a = 0.66 eV) and the extrapolated RT conductivity is $\sigma_{(298\,K)} = 8 \times 10^{-11}\ S\,cm^{-1}$. Such a value is consistent with previously published data [19] and can be attributed to the Na^+ mobility. One should note that, for this matrix, temperature measurements could be performed only up to 350 °C, where it showed already a good conductivity, since melting of the material was registered above 400 °C. This is much different from the LiBPO sample which is stable up to over 1000 °C and where conductivity could not be observed below 475 °C. The softer nature of the NaBPO matrix may imply a weaker bonding and thus a stronger ionic mobility, resulting in an enhancement of the conductivity.

3.5. Electrochemical characterizations

The first cycle galvanostatic response of the two modified composites (SnLiBPO and SnNaBPO) and the reference composite (SnBPO) are shown in Fig. 7. The SnBPO composite shows the highest loss with an irreversible capacity of about 245 mAh g^{-1} after the second discharge/charge cycle. This is anyway around one third of the irreversible capacity value of the amorphous tin composite oxide [7,8]. The electrochemical behavior is sensibly improved using more conducting matrixes for the β-Sn dispersion.

The lithium consumption at 1.5 V vs. Li^+/Li^0 has been attributed to the interfacial Sn^{II} reduction [9,14]. More than the consumption of lithium due to this reduction, the three samples exhibit electrolyte reduction which can be due to the formation of a SEI layer on conducting carbon at around 0.75 V vs Li^+/Li^0 [20]. The phenomena are probably contemporary with the formation of the first, lithium-poor, Li–Sn alloys [14].

The SnLiBPO sample exhibits the best performances. It has been possible to lithiate/de-lithiate additional 0.3 Li^+ per atom of tin in the composite compared to the reference. Some activation/kinetic effects also take place during the galvanostatic test of this sample. The extent of the Sn^{II} reduction is in the middle between what we observed for the reference and the SnNaBPO composites. This is related to the smaller amount of Sn^{II} specie present in the composite (see "effective fraction", Table 2).

In the case of the SnNaBPO sample, a lower capacity can be obtained due to the higher weight of the matrix herself. The superior Na^+ conductivity is probably not influent on the electrochemical results but the interface restructuration taking place during the first discharge could modify the NaBPO glass by the addition of some mobile Li^+.

A deeper study in this direction is being carried on in our laboratory.

4. Conclusion

In conclusion, we have analyzed the influence of dispersion matrix on electrochemical performances in tin-based composite materials. The composites are synthesized by *ex situ* dispersion of micrometric tin in crystallized BPO_4, Li-doped BPO_4 and amorphous Na-substituted BPO_4 matrixes. ^{119}Sn Mößbauer spectroscopy shows the presence of starting β-Sn and the formation of a new Sn^{II} species. The proportion of Sn^{II} is reduced at 26% in the case of Li^+ and 11% in the case of Na^+ with respect to the reference $SnBPO_4$ (44%).

The effect of incorporation of Li^+ and Na^+ in the starting matrix is also to increase the conductivity, an important parameter for fast electrochemical cycling in this material. The diminution of interfacial Sn^{II} has the consequence of diminishing the irreversible capacity during the first cycle. The present work improves the understanding of the relationship between interface structure and electrochemical performances, more particularly irreversible capacity; even if a number of points remain unclear, such as the influence of cycling rate and the possible "structuration" of the composite during the first or following cycles.

Acknowledgements

The financial support of the agreement CNES-Région Languedoc Roussillon N° 07-011380 as well as the contract ANECDOTE ANR-07-Stock-E-03-02 are largely appreciated. The authors want to thank Dr M. Womes, Dr P.E. Lippens and Dr. Prof. L. Stievano for the discussions on Mößbauer results, Mr. C. Grille and Mr. F. Fernandez for the SEM imaging and EDX analyses.

References

[1] P. Poizot, S. Laruelle, S. Grugeon, L. Dupont, J.-M. Tarascon, Nature 407 (2000) 496.
[2] Y. Idota, T. Kubota, A. Matsufuji, Y. Maekawa, T. Miyasaka, Science 276 (1997) 1395.
[3] I.A. Courtney, J.R. Dahn, J. Electrochem. Soc. 144 (1997) 2045.
[4] K. Furuya, K. Agawa, Y. Mineo, A. Matsufuji, J. Okuda, T. Erata, J. Phys. Condens. Mater. 13 (2001) 3519.
[5] I.A. Courtney, R.A. Dunlap, J.R. Dahn, Electrochem. Acta 45 (1999) 51.
[6] J. Chouvin, C.P. Vicente, J. Olivier-Fourcade, J.-C. Jumas, B. Simon, P. Biensen, Solid State Sci. 6 (2004) 39.
[7] F. Robert, P.E. Lippens, J. Olivier-Fourcade, J.C. Jumas, M. Morcrette, J. Power Sources 146 (2005) 492.
[8] D.E. Conte, A. Aboulaich, F. Robert, J. Olivier-Fourcade, J.-C. Jumas, C. Jordy, P. Willmann, J. Solid State Chem., doi:10.1016/j.jssc.2009.10.015, in press.
[9] A. Aboulaich, M. Mouyane, F. Robert, P.-E. Lippens, J. Olivier-Fourcade, P. Willmann, J.-C. Jumas, J. Power Sources 174 (2007) 1224.
[10] A. Aboulaich, F. Robert, P.-E. Lippens, J. Olivier-Fourcade, P. Willmann, J.-C. Jumas, Hyperfine Interact. 167 (2006) 733.
[11] C. Frontera, J. Rodríguez-Carvajal, Physica B 335 (2003) 219.
[12] W. Kündig, Nucl. Inst. Methods 75 (1969) 336.
[13] J.A. Lee, G.V. Raynor, Proc. Phys. Soc., Lond. B67 (1954) 737.
[14] F. Robert, P.-E. Lippens, J. Olivier-Fourcade, J.-C. Jumas, F. Gillot, M. Morcrette, J.-M. Tarascon, J. Solid State Chem. 180 (2007) 339.
[15] P.E. Lippens, Phys. Rev. B 60 (7) (1999) 4576.
[16] E.M. Kelder, M.J.G. Jak, F. de Lange, J. Schoonman, Solid State Ionics 85 (1996) 285.
[17] M.J.G. Jak, E.M. Kelder, Z.A. Kaszkur, J. Pielaszek, J. Schoonman, Solid State Ionics 119 (1999) 159.
[18] S. Lanfredi, M.A. de Lima Nobre, Mater. Res. 6 (2) (2003) 157.
[19] P.S. Amantha, K. Hariharan, Mater. Chem. Phys. 89 (2005) 428.
[20] J.Z. Li, H. Li, Z.X. Wang, L. Chen, X.J. Huang, J. Power Sources 107 (2002) 1.